JOURNAL OF GEOPHYSICAL RESEARCH, VOL. 94, NO. C4, PAGES 4959–4970, APRIL 15, 1989

A Numerical Model of the Atmospheric Boundary Layer Over a Marginal Ice Zone

LAKSHMI H. KANTHA[1] AND GEORGE L. MELLOR

Atmospheric and Oceanic Sciences Program, Princeton University, Princeton, New Jersey

A two-dimensional, multilevel model for simulating changes in the atmospheric boundary layer across a marginal ice zone is described and applied to off-ice, on-ice, and along-ice edge wind conditions. The model incorporates a second-moment closure for parameterizing the intensification and suppression of turbulent mixing in the boundary layer due to stratification effects. For off-ice winds, as the atmospheric boundary layer passes from cold smooth ice onto warm open water, the onset of intense convection raises the inversion. Over the transition zone of rough rafted ice with open leads, the shear stress on the ice cover increases significantly before dropping down to the downstream values over water. Such nonmonotonic surface stress could be the cause of divergence of sea ice near the ice edge in a marginal ice zone. These results are in agreement with the one-layer model simulations of off-ice winds by Overland et al. (1983). For on-ice wind conditions, as the warm flow in the boundary layer encounters the cold ice conditions, the resulting stable stratification could rapidly suppress the turbulence in the boundary layer, leading to the development of a shallow inversion and an associated jet. When the wind is predominantly along the ice edge, the temperature contrast between the open water and the ice could produce a thermal front at the ice edge in the boundary layer with strong associated turbulence. More observations are needed to verify these model predictions. Nevertheless, these model results suggest that it is important to account for the changes in the characteristics of the atmospheric boundary layer across the marginal ice zone in our attempts to understand the behavior of the ice cover in these regions.

1. INTRODUCTION

The interactions between the atmosphere, the ocean, and the ice cover are particularly strong in a marginal ice zone (MIZ). It is therefore preferable to study the coupled system as a whole rather than each medium in isolation, in order to further our understanding of this important part of our environment. The complexity of the interactions between the atmosphere and the ocean, especially when mediated by the ice cover, makes such a study rather difficult. One promising approach is through process studies using a numerical model of the coupled system that accounts for the dynamic and thermodynamic interactions between all three media. Unfortunately, it will be a while before reliable coupled models, tested against observations, can be used routinely for this purpose. One of the principal problems is, of course, the dearth of suitable data sets that can be used for a meaningful verification of the capabilities of such models. Despite the increased attention being paid to the Arctic and the Antarctic in recent years, through multinational efforts such as the Marginal Ice Zone experiments (MIZEX), our empirical data base is still rather scanty. Simultaneous observations of the characteristics of all three media, essential to the success of a coupled model, are very few.

Nevertheless, the necessity of studying the coupled system has been increasingly recognized in recent years. Efforts are now underway to develop and test coupled atmosphere-ice-ocean models for these regions. As part of one such effort, we have developed a coupled ice-ocean model and an atmospheric boundary layer model and are testing both models before coupling them to each other. Two-dimensional versions of both these models have simulated flows in a marginal ice zone. The results of the ice-ocean model will be reported elsewhere [*Kantha and Mellor*, 1989; *Mellor and Kantha*, 1989]. In this paper we will present the results of the application of the two-dimensional atmospheric boundary layer model to off-ice, on-ice, and along-ice edge wind conditions in a MIZ.

The modifications of the atmospheric boundary layer by a MIZ under off-ice wind conditions have been simulated by *Overland et al.* [1983] using a single-layer, two-dimensional model of the boundary layer. This study demonstrates the strong influence of the changes in the roughness of and the heat transfer from the underlying surface on the structure of the boundary layer. It shows that as the wind flows off the smooth ice and onto open water over a rough MIZ, the wind speed first decreases but then increases over the MIZ. This suggests an atmospheric mechanism for ice edge convergence and divergence, which might act in concert with the oceanic drag mechanism suggested by *McPhee* [1983]. *Reynolds* [1984] made a more detailed study that included the effects of clouds, surface heat flux, and radiative cooling in the MIZ and showed that most of the observed variations in the atmospheric boundary layer (ABL) over the Bering Sea MIZ made in 1981 can be attributed to the increased roughness over the MIZ and the increased heat flux over the open ocean. He found that the heat flux in the MIZ itself and cloud processes did not alter the results significantly. He also used a single-layer or slab model for this study. His results emphasize the importance of ice surface roughness variations on ice drift in a MIZ.

While a slab model can capture the essence of the boundary layer modifications over a MIZ during off-ice conditions, if not the details of its vertical structure, it is not appropriate to the study of more general cases including on-ice wind conditions. This has led to the increased use of a multilevel model over the MIZ [*Bennett and Hunkins*, 1986; *Overland*,

[1]Now at Institute for Naval Oceanography, Stennis Space Center, Mississippi.

Paper number 89JC00076.
0148-0227/89/89JC-00076$05.00

1988]. *Overland* [1988] has used a multilevel, one-dimensional model to test the sensitivity of the geostrophic drag coefficient to various atmospheric parameters over a MIZ. This study complemented his earlier comprehensive review [*Overland*, 1985] of the drag coefficient estimates and measurements over sea ice. *Bennett and Hunkins* [1986] have used a linear, two-dimensional, multilevel model to simulate on-ice wind conditions over the Weddell Sea MIZ corresponding to the observations of *Andreas et al.* [1984]. However, there appear to have been no model studies of along–ice edge wind conditions in a MIZ, a situation that could also lead to significant modifications of the atmospheric boundary layer structure (J. Overland; personal communication, 1988). A multilevel model is essential for such studies.

There are few observations of the atmospheric boundary layer over sea ice, but the situation is improving steadily. The various large-scale international data collection efforts such as the Marginal Ice Zone experiments have improved our knowledge of the ice edge processes in general and the behavior of the atmospheric boundary layer in particular. For example, field observations reported by *Anderson* [1987], *Guest and Davidson* [1987] and *Kellner et al.* [1987] over the Greenland Sea MIZ during the 1983 MIZEX have again emphasized the strong variations in the roughness characteristics of the ice surface in a MIZ and their consequent influence on the drag felt by the atmospheric boundary layer. The surface drag coefficient has been found to be correlated rather well with ice concentration and with the roughness and size of ice floes.

It appears therefore that the most important factors in the evolution of the atmospheric boundary layer over a MIZ are the strong variations in the ice surface roughness and the strong disparity in the heat transfers from the ice surface and the ocean to the atmosphere. We therefore concentrate on these features in our multilevel atmospheric boundary layer model and ignore the liquid water vapor thermodynamics for the time being. While the atmosphere is dry and therefore somewhat simplified, the turbulent mixing processes that are essential for accounting for the changes of roughness and heat flux on the structure of the boundary layer are parameterized using second-moment closure. The model is two-dimensional and ignores the variations along the ice edge, thus assuming that the scale of variations along the ice edge is larger than that across the ice edge.

The paper is organized as follows. Section 2 deals with a description of the boundary layer model, and Section 3 discusses the relevant numerical details. Section 4 details the results of its application to off-ice, on-ice, and along–ice edge wind conditions. Section 5 contains concluding remarks.

2. The Numerical Model

The numerical model for the atmospheric boundary layer is similar to the ocean model described by *Blumberg and Mellor* [1983] and *Oey et al.* [1985]. Many of the numerical details of the ocean model are given by *Blumberg and Mellor* [1987]. The atmospheric model also uses second-moment closure for parameterizing vertical mixing. The governing equations and the method of solution are similar. The model is based on fully nonlinear hydrodynamic equations of motion for conservation of mass, momentum, and enthalpy; it simplified, however, by the use of incompressible, hydrostatic, and Boussinesq approximations. The atmosphere is considered to be dry and the perfect gas relation $p = \rho RT$, where p is the pressure, R is the gas constant, ρ is the density, and T is the temperature, is used to reduce the governing equations for ensemble mean quantities to

$$\nabla \cdot \mathbf{V} + \frac{\partial w}{\partial z} = 0 \tag{1}$$

$$\frac{\partial \mathbf{V}}{\partial t} + \mathbf{V} \cdot \nabla \mathbf{V} + w \frac{\partial \mathbf{V}}{\partial z} + \mathbf{f} \times \mathbf{V} = -\frac{\Theta}{\Theta_0} \nabla \pi + \frac{\partial}{\partial z}\left(K_M \frac{\partial \mathbf{V}}{\partial z}\right) + \mathbf{F} \tag{2}$$

$$\frac{\partial \pi}{\partial z} = -g \frac{\Theta_0}{\Theta} \tag{3}$$

$$\frac{\partial \Theta}{\partial t} + \mathbf{V} \cdot \nabla \Theta = \frac{\partial}{\partial z}\left(K_H \frac{\partial \Theta}{\partial z}\right) + F_\Theta \tag{4}$$

$$\frac{\Theta}{\Theta_0} = \left(\frac{T}{T_0}\right)\left(\frac{p}{p_0}\right)^{-(\gamma-1)/\gamma} \tag{5}$$

$$\pi = C_p \Theta_0 \left(\frac{p}{p_0}\right)^{(\gamma-1)/\gamma} \tag{6}$$

Equation (3) is the hydrostatic approximation, while equations (5) and (6) define a potential temperature Θ and a pressure term π. The quantity $\mathbf{f}$ is the Coriolis vector, $\mathbf{V}$ is the horizontal velocity vector, and ∇ is the horizontal gradient operator. The quantity γ is the ratio of specific heats at constant pressure C_p and constant volume C_v, while $R = C_p - C_v$. The subscript 0 denotes a reference state. The quantity g is the gravitational acceleration; z is the vertical coordinate, and w is the vertical velocity. The quantities K_M and K_H denote vertical eddy diffusivities for turbulent mixing of momentum and heat. The horizontal diffusion terms $F_{x,y}$ and F_Θ are given by

$$F_x = \frac{\partial}{\partial x}\left(2A_M \frac{\partial U}{\partial x}\right) + \frac{\partial}{\partial y}\left[A_M\left(\frac{\partial U}{\partial y} + \frac{\partial V}{\partial x}\right)\right] \tag{7}$$

$$F_y = \frac{\partial}{\partial y}\left(2A_M \frac{\partial V}{\partial y}\right) + \frac{\partial}{\partial x}\left[A_M\left(\frac{\partial U}{\partial y} + \frac{\partial V}{\partial x}\right)\right] \tag{8}$$

$$F_\Theta = \frac{\partial}{\partial x}\left(A_H \frac{\partial \Theta}{\partial x}\right) + \frac{\partial}{\partial y}\left(A_H \frac{\partial \Theta}{\partial y}\right) \tag{9}$$

where the quantities A_M and A_H denote horizontal diffusivities. The vertical eddy coefficients K_M and K_H are calculated from

$$K_{M,H} = qlS_{M,H} \tag{10}$$

where S_M and S_H are stability functions, prescribed from the level $2\frac{1}{2}$ model of the Mellor-Yamada second-moment closure hierarchy [*Mellor and Yamada*, 1982]:

$$S_M\,[6A_1A_2G_M] + S_H\,[1 - 3A_2(4A_1 + B_2)G_H] = A_2 \tag{11}$$

$$S_M\,[1 + 6A_1^2G_M - 9A_1A_2G_H] - S_H\,[3A_1(4A_1 + 3A_2)G_H] = A_1\,(1 - 3C_1) \tag{12}$$

$$G_M = \frac{l^2}{q^2}\left[\left(\frac{\partial U}{\partial z}\right)^2 + \left(\frac{\partial V}{\partial z}\right)^2\right] \tag{13}$$

$$G_H = -\frac{l^2}{q^2}\frac{g}{\Theta_0}\frac{\partial \Theta}{\partial z} \tag{14}$$

The turbulence velocity q and length scale l are given by equations

$$\frac{\partial}{\partial t}(q^2) + \mathbf{V}\cdot\nabla q^2 + w\frac{\partial q^2}{\partial z} = \frac{\partial}{\partial z}\left[qlS_q\frac{\partial}{\partial z}(q^2)\right] + 2(P_s + P_b - \varepsilon) + F_q \quad (15)$$

$$\frac{\partial}{\partial t}(q^2 l) + \mathbf{V}\cdot\nabla(q^2 l) + w\frac{\partial}{\partial z}(q^2 l) = \frac{\partial}{\partial z}\left[qlS_1\frac{\partial}{\partial z}(q^2 l)\right] + E_1 l(P_s + E_3 P_b) - l\varepsilon\left[1 + E_2\left(\frac{l}{kL}\right)^2\right] + F_l \quad (16)$$

where

$$\varepsilon = \frac{q^3}{B_1 l} \quad (17)$$

$$P_s = K_M\left[\left(\frac{\partial U}{\partial z}\right)^2 + \left(\frac{\partial V}{\partial z}\right)^2\right] \quad (18)$$

$$P_b = -K_H\frac{g}{\Theta_0}\frac{\partial\Theta}{\partial z} \quad (19)$$

The symbols P_s and P_b denote shear and buoyancy production of turbulence kinetic energy, and ε denotes its viscous dissipation; l is the turbulence length scale, a measure of the scale of the energy-containing eddies that contribute to the cascade process.

The symbols F_q and F_l, denote horizontal mixing terms with expressions similar to that of F_Θ except that q^2 and $q^2 l$ replace Θ; L is a measure of the distance from a solid surface. The constants k, A_1, A_2, B_1, B_2, C_1, E_1, E_2, E_3, S_q and S_l are 0.4, 0.92, 0.74, 16.6, 10.1, 0.08, 1.8, 1.33, 1.0, 0.2, and 0.2, respectively, and are assumed to be universal constants applicable to all turbulent flows. The reader is refered to *Mellor and Yamada* [1982], *Markatos* [1986], and *Rodi* [1987] for recent reviews of second-moment closure of turbulence.

It is also necessary to impose realizability conditions on G_M, G_H, and l such that

$$G_H \le 0.0288 \quad (20a)$$

$$G_M \le 0.45 - 15.0\,G_H \quad (20b)$$

$$l \le 0.5qN^{-1} \quad (20c)$$

where N is the buoyancy frequency.

The first condition assures that all variances remain positive-definite, while the second defines the limits of validity of Rotta hypothesis under highly anisotropic turbulence conditions. It appears that in stably stratified flows the maximum size of the eddies that participate in the cascade process and therefore contribute to turbulent mixing is limited by stratification. We therefore impose an upper bound on the turbulence length scale l according to (20c). A useful consequence of this upper bound on l is that there is no leakage of turbulence kinetic energy above a strong capping inversion. Calculated results generally are not overly sensitive to the constants in (20).

An advantage of this model is a more realistic parameterization of turbulent mixing processes in the boundary layer. A slab model, on the other hand, assumes that the mixing coefficients in the boundary layer are essentially infinite; also, the entrainment rate at the inversion needs to be parameterized from data, thus introducing empiricism into the formulation, although at a strong inversion the model results appear to be rather insensitive to this prescription [*Overland et al.*, 1983]. The assumption of a well-mixed, homogeneous boundary layer, although often invoked in both the oceanic and atmospheric mixed layer models, is an approximation whose degree of validity depends on the flow conditions being simulated. Thus, for example, while it may be adequate for a convective mixing such as that encountered by the boundary layer as it flows off the ice onto warm open water, it is a poor approximation for the opposite situation, where a warm layer flows off the ocean onto cold ice surface and mixing may be inhibited by strong stable stratification. Both situations occur in a MIZ, and the present model is equally applicable to both on-ice and off-ice conditions.

The above equations have been recast in sigma coordinates, so that the number of levels in the vertical is independent of the topography of the underlying surface. However this feature is not essential to the current application to a MIZ. (Sigma coordinates are useful, however, in simulating flow over topography.) The mass and momentum conservation equations are integrated in the vertical, and the resulting external mode equations are solved at smaller steps dictated by the speeds of propagation of barotropic disturbances. The internal mode equations are solved at larger time steps dictated by baroclinic modes. The interested reader is referred to *Blumberg and Mellor* [1987] for relevant details. We note here that in the application of the above atmospheric boundary layer model to a MIZ, we orient the y axis along the ice edge and put $\partial\phi/\partial y \equiv 0$, where ϕ is any property.

3. Numerical Details

A primary objective of this study was to be able to compare the performance of this model with that of the highly simplified slab models for the off-ice winds over a MIZ. Therefore the principal model parameters for off-ice simulations were chosen to correspond to those of *Overland et al.* [1983], although studies of model sensitivity to some of these parameters were also undertaken. For example, we chose a horizontal resolution of 2 km to conform to the simulations of Overland et al. so that a direct comparison with their results for off-ice conditions would be feasible. Similarly, the width of the simulated zone is 160 km. A 2-km-thick atmospheric column is simulated with 24 vertical levels. The computational grid is therefore 80 × 24. Because of the low inversion heights in ice-covered regions (typically a few hundred meters), it should not be necessary to simulate a thicker slice of the atmosphere. The inversion height is around 450 m in the current simulations, and the vertical resolution was arranged to be 20 m in the vicinity of the inversion, decreasing to 300 m near the top (see Table 1). The coarsest resolution in the mixed layer itself is 75 m. The resolution near the bottom is much finer to resolve the constant flux region, with the bottommost grid 5 m thick. This facilitates matching the velocity and potential temperature at this grid point to a logarithmic layer because the assumption of the validity of log law for both velocity and temperature profiles is a fairly good approximation at the bottommost grid point. The atmosphere is dry, and the Coriolis parameter corresponds to a latitude of 60°N.

TABLE 1. Model Levels

Sigma Level	Height, m
1	2000
2	1700
3	1400
4	1100
5	800
6	580
7	560
8	540
9	520
10	500
11	480
12	460
13	440
14	420
15	400
16	350
17	300
18	225
19	150
20	75
21	35
22	15
23	5
24	0

The ice and ocean surface temperatures are taken as -11°C and -1°C, and the lapse rate above the inversion is taken as 10° C km^{-1}. The geostrophic wind above the inversion is also taken as 13 m s^{-1}. These values correspond to the off-ice simulations of Overland et al. The drag coefficients C_D for smooth ice, rough ice, and open water are also taken as 0.002, 0.0038, and 0.002, respectively, to correspond to their values (see their Table 2) for all simulations described in this paper. In simulations of the MIZ (case 3 of Overland et al. and of this paper), smooth ice cover in the interior is assumed to give way to a rough ice cover through a transition zone where C_D increases linearly from the smooth value to the rough value.

The heat transfer coefficient C_H over the ocean is taken as 0.002 irrespective of the flow direction. We assume that there is no heat flow from the ocean to the atmosphere through the ice cover. This implies that over the interior smooth ice, where no leads are assumed to exist, no heat flux from the ocean to the atmosphere is possible. On the other hand, leads are assumed to exist over 30% of the ice cover in the rough and transition zones, allowing the ocean to transfer heat to the atmosphere. However, when the ABL is warmer than the ice surface, we assume that the ABL transfers heat to the ice, while the ice surface temperature remains at -11°C. It is this heat flux that is responsible for quenching the turbulence in the ABL when it flows onto the cold ice surface, resulting in the formation of low-level inversions. If there were no such heat flux from the ABL to the ice, turbulence in the ABL would not be not quenched; instead it would adjust to the mechanical mixing produced by the roughness of the ice surface. The roughness scales for velocity and temperature required by the model are prescribed so as to yield the above mentioned drag and heat transfer coefficients, and therefore they are not necessarily equal to each other. The velocity and potential temperature profiles are matched to the classical, logarithmic laws of the wall relations for both velocity and temperature at the bottommost grid point.

The horizontal diffusivities A_M and A_H are prescribed to be 8500 m^2 s^{-1}. The vertical mixing coefficients are determined from second-moment turbulence closure as described earlier.

The flow is from right to left; inflow conditions, such as the velocity and temperature distributions, are prescribed and held fixed. The air column up to the level of inversion is assumed to be initially at the same temperature as the underlying surface. Initially, the inversion height is assumed to be 450 m.

Except for the case of along–ice edge winds, the model was spun up for a day with homogeneous terrain corresponding to the inflow terrain. The ABL achieved equilibrium rapidly within a few tens of kilometers from the inflow boundary, and steady state was attained during this period. Conditions obtained near the outflow boundary from this spin-up were then prescribed as upstream boundary conditions in the simulations of various off-ice and on-ice MIZ conditions, and the model was run for another day. This procedure is equivalent to having an additional 160 km of upstream terrain conditions and obviates the need to have a larger domain in the MIZ simulations. The prescribed upstream ABL structure is thus also consistent with the classical results of flow over a homogeneous terrain, and minimal adjustment takes place at the upstream open boundary. For the along–ice edge simulations, this procedure was not feasible, and one can discern some local adjustment near the inflow boundary (for example, Figure 19).

4. Model Results

The model simulations described here follow closely the simulations of *Overland et al.* [1983]. In particular, the different cases considered correspond to their different cases. For example, case 1 refers to the situation where smooth ice adjoins open water, whereas case 3 refers to the MIZ situation when smooth interior ice gives way to open water through a transitional and a rough ice zone.

Three series of simulations were made corresponding to off-ice, on-ice and nearly along–ice edge wind conditions. The inversion conditions aloft were chosen to be the same in all three series, and the inversion strengths were also chosen to be roughly similar and representative of the MIZ. In all these simulations, boundary values are prescribed at the inflow boundaries, while at the outflow boundaries, upwind advection is prescribed, so that temperature is advected out from the interior. At the top of the atmosphere, geostrophic velocity and potential temperature are prescribed and held fixed; zero gradient conditions are imposed on turbulence velocity and length scales. Figure 1 shows schematically the relevant conditions for all three series of simulations.

4.1. *Off-Ice Wind Conditions*

Overland et al. [1983] considered three cases of off-ice wind conditions. Case 1 involves flow from a smooth ice interior to open water which begins 60 km from the inflow boundary. Since the drag coefficient is the same for both the ice and the open water, this case simulates changes in the ABL structure to increased heat transfer from the underlying surface.

Case 2 involves flow from rough ice to open water. Therefore the ABL is subject to increased heat transfer from as well as decreased roughness of the underlying surface.

Case 3 considers a 30-km-wide smooth interior ice zone followed by a 10-km-wide transition zone and a 20-km-wide rough ice zone adjoining open water and roughly simulates conditions in a MIZ. In this case, the ABL feels both increasing heat transfer as well as increasing roughness as it flows over the MIZ before encountering open water where the roughness decreases but heat transfer intensifies.

In all these cases the ABL temperature at the inflow boundary is taken as −11°C, the same as that of the ice surface, and the jump at the base of the inversion (referred to hereinafter as inversion strength) is taken as 7°C. We present the results of all three off-ice simulations with the current model and compare them with those of *Overland et al.* [1983].

Figures 2 and 3 show the model results for case 1, the former showing the potential temperature and turbulence kinetic energy (TKE) distributions in the lower 800 m of the atmosphere, while the latter displays the cross–ice edge (U) and along–ice edge (V) velocities. Figure 2 shows the rapid increase of the ABL temperature once it encounters open water. The inversion is lowered slightly because of flow acceleration due to positive temperature gradient at the ice edge before beginning to rise slowly over the open water owing to erosion from strong convective mixing. The strong inversion, however, inhibits more drastic changes in ABL thickness. Turbulence over the ice surface is mechanically generated. However, as the stability in the ABL changes from neutral over ice to strong destabilizing over the warm water, intense convection sets in, as is indicated by the TKE distribution in Figure 2. The cross–ice edge velocity is also more uniform over water, with most of the gradient confined to the immediate vicinity of the ocean surface owing to the intense mixing in the ABL; it is less uniform over ice (Figure 3). There is also a stronger jump in the along–ice edge velocities across the inversion over water than over ice.

Figures 4 and 5 show the corresponding results for Case 2. A difference from Case 1 is higher turbulence intensities over ice (Figure 4) due to rougher surface conditions. The lowering of the inversion near the ice edge is slightly higher. The rate of increase in ABL temperature over water is however practically the same, while the velocity fields also exhibit very little change (Figure 5).

Potential temperature and TKE distributions for Case 3 are shown in Figure 6. Here the ABL temperature begins to increase immediately after the flow moves off the interior smooth ice, because of the heat transfer from open leads in the transition zone. Because of this as well as the increased roughness of the ice surface, the turbulence intensities in the ABL nearly double. Once open water is reached, intense convection more than compensates for decreased roughness and turbulence in the ABL intensifies strongly. Figure 7 shows the corresponding velocity distribution in the ABL.

Figures 8*a*, 8*b*, and 8*c* compare the ABL temperature, cross–ice edge velocity, and ABL thickness obtained from the present simulations with those of *Overland et al.* [1983] for all three off-ice cases. These are the dependent variables in a slab model. In the current model, since a mixed layer is by no means perfectly mixed even under strongly unstable conditions, especially with respect to momentum, the mixed layer height was defined as the height at which the nearly uniform temperature at the bottom of the inversion increases by 0.1°C. The mixed layer temperature and velocity were taken as those corresponding to the nearly uniform conditions at the top of the mixed layer.

It is evident from Figure 8 that there is a good agreement between the current model and the slab model of *Overland et al.* [1983]. The minor differences can be attributed partly to the definition of the various quantities in the current model. But primarily, the differences are related to the fact that a slab model assumes that the entire ABL responds to changes in the bottom boundary conditions (mixing intensity is essentially infinite) and therefore tends to exaggerate the changes in the ABL. The current model allows for development of internal boundary layers that result from finite, realistic mixing coefficients. Nevertheless, the current simulations demonstrate the utility of slab models for simulating off-ice wind conditions and confirm the conclusions reached by Overland et al. As is shown by Figure 8*c*, the ABL velocity over the MIZ drops initially but begins to increase well before the ice edge is reached.

Figure 9 shows the cross–ice edge kinematic shear stress as a function of distance from the ice edge for all three cases. It is clear that for the case 3 simulation, the shear stress increases sharply to well above the downstream values over water before decreasing to downstream values (there is a small overshoot because of the sharp change in properties at the ice edge, due to a somewhat inadequate horizontal mixing coefficient). This peak in the surface stress could provide the necessary atmospheric mechanism for ice rafting and ice edge divergence in a MIZ, suggested originally by Overland et al.

Figure 10 displays the ABL height and the increase in the ABL temperature across the MIZ for four different simulations corresponding to the case 3 simulation described previously. Curve 1 denotes the simulation with the approaching ABL temperature of −11°C and an inversion strength of 7°C. Curves 2 and 3 denote simulations in which the inversion strength is 2°C and 12°C, respectively, but the ABL temperature is kept at −11°C, while curve 4 corresponds to a simulation in which the ABL temperature is lowered to −21°C, keeping the inversion strength at 7°C. These experiments demonstrate that as long as the inversion strength is large enough not to be eroded completely by convective heating, the change in the mixed layer height across the MIZ is relatively insensitive to the strength of the inversion. The rate of increase of ABL temperature is also relatively insensitive to inversion strength. However, the mixed layer heats up more rapidly when the ice-water temperature contrast is increased as is shown by curve 4.

4.2. *On-Ice Wind Conditions*

The second series of simulations involves on-ice wind conditions. We present only two cases, the first one with flow from open water onto rough ice conditions. In this case, the ABL feels a step change in the temperature and roughness of the underlying surface. In the second simulation, the flow crosses from open water onto the MIZ; in the process it flows over a 20-km-wide rough ice zone followed by a 10-km-wide transition zone before moving onto smooth ice. The ABL therefore feels variable roughness as well as a step change in surface temperature. The inflow temperature in the ABL is the same as the water temperature, −1°C. The inversion height is prescribed as 450 m and the inversion strength as 2°C (not 7°C as in the previous case) at the inflow

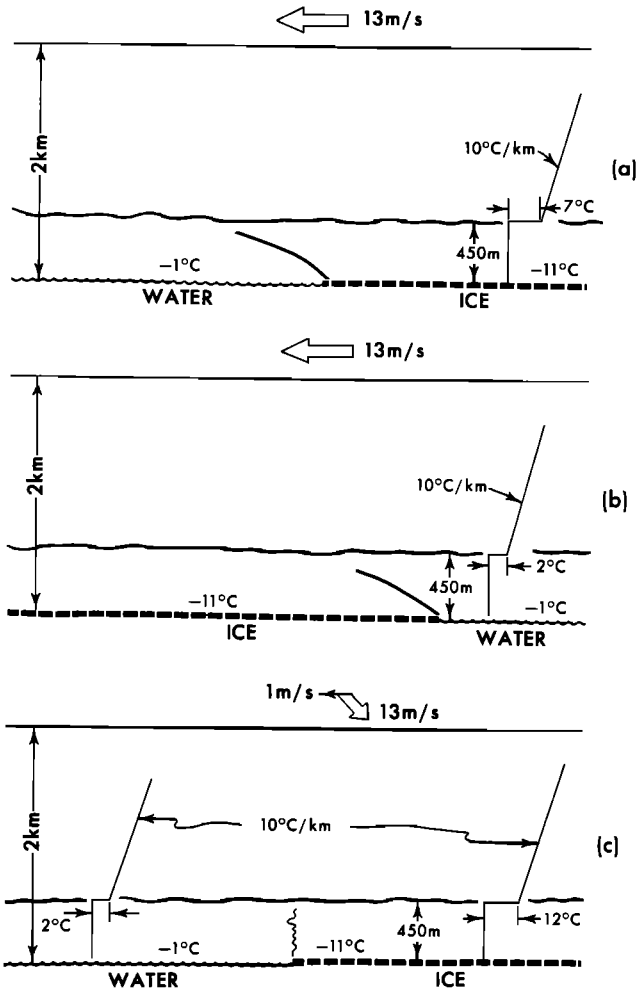

Fig. 1. Schematics of the simulations for (*a*) off-ice, (*b*) on-ice, and (*c*) along-ice edge wind conditions over the MIZ. As described in the text, several runs that correspond to different ice cover conditions are undertaken for each of these cases. Figure 1*c* shows the condition for the first case of along-ice edge simulations; for the second case, the ice is on the left-hand side while the open water is on the right-hand side.

boundary, so that the conditions aloft are roughly similar to those in the previous series.

Figure 11 shows the potential temperature and TKE distributions corresponding to case 2 of on-ice flow conditions, i.e., flow from open water onto rough ice. As the warm air column encounters the cold ice surface it begins to transfer its heat to the underlying surface, resulting in strong stable stratification that suppresses turbulence in the ABL. Turbulence collapses over most of the ABL and is instead confined to the immediate vicinity of the ground. It is shear-generated and has to work against gravitational forces, a situation somewhat analogous to the transition from daytime heating to nocturnal conditions in the ABL at lower latitudes. A shallow inversion (a few tens of meters) develops close to the ice surface as can be seen from both temperature and TKE distributions (Figure 11). The shallow inversion is associated with a strong jet reminiscent of the nocturnal jet in the atmosphere (Figure 12). The height of the inversion can be expected to be a strong function of the magnitude of the heat flux from the ABL to the ice. The along-ice edge velocities also build up in the low-level

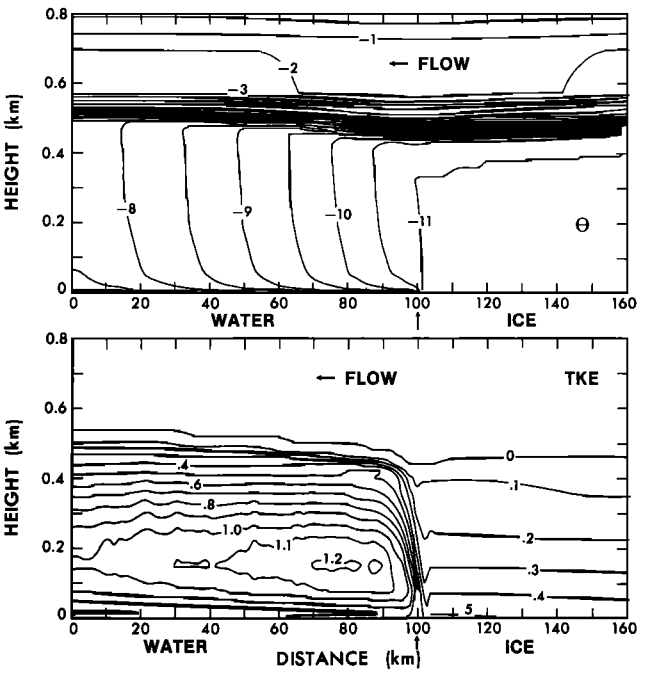

Fig. 2. (Top) Potential temperature (in degrees Celsius) and (bottom) turbulence kinetic energy (in $m^2 s^{-2}$) in the lower 800 m of the atmospheric boundary layer for case 1 off-ice wind conditions (flow from smooth ice onto open water). The flow is from right to left. Note the intense convective activity over open water resulting in rapid heating and intense turbulence in the boundary layer. The vertical arrow near the abscissa denotes the ice edge, and the horizontal one near the top denotes the principal flow direction.

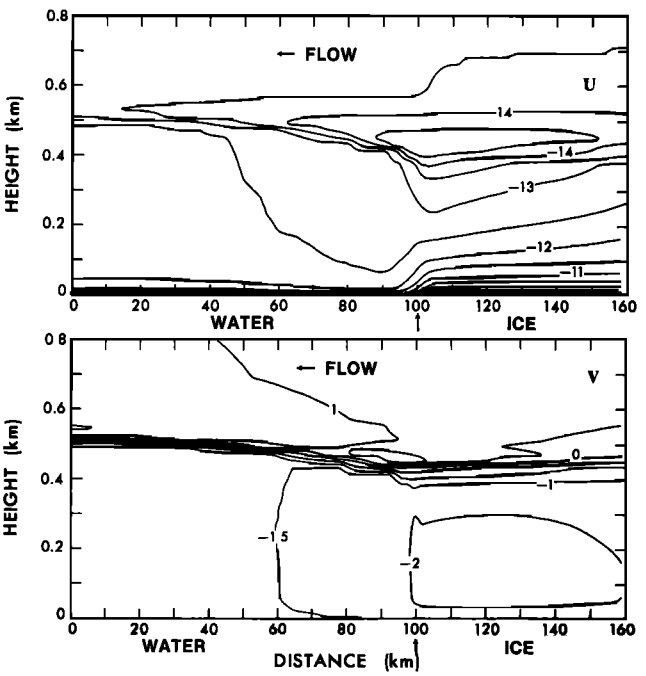

Fig. 3. (Top) Cross-ice edge and (bottom) along-ice edge velocities (in meters per second) in the lower 800 m of the atmospheric boundary layer for case 1 off-ice wind conditions (flow from smooth ice onto open water). The flow is from right to left. Note the change in the velocity structure across the ice edge. The vertical arrow near the abscissa denotes the ice edge, and the horizontal one near the top denotes the principal flow direction.

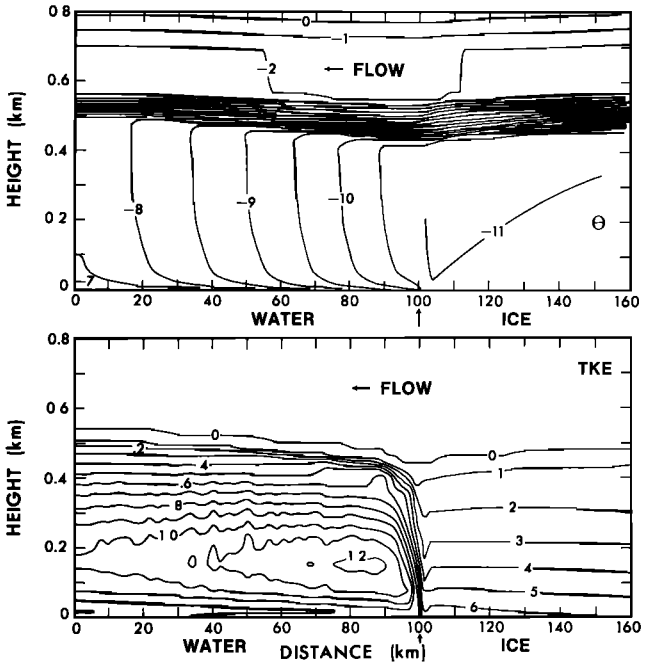

Fig. 4. Potential temperature and turbulence kinetic energy as in Figure 2, but for case 2 off-ice winds (flow from rough ice onto open water).

inversion. The original inversion is also lowered somewhat because of the acceleration of the flow in the entire ABL.

Figures 13 and 14 display the results corresponding to case 3. This case simulates a situation where the initially off-ice winds have shifted direction and have begun to flow on-ice. Although there are some noticeable differences due to the differences in roughness of the underlying surface and the heat exchange between the two cases, the behavior of the ABL is substantially similar. It is noteworthy that turbulence actually increases in intensity before being extinguished over

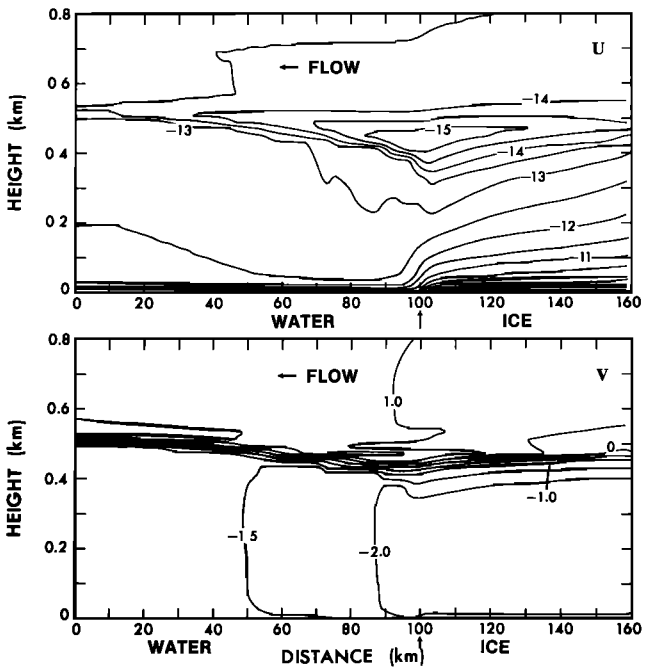

Fig. 5. Cross–ice edge and along–ice edge velocities as in Figure 3, but for case 2 off-ice winds (flow from rough ice onto open water).

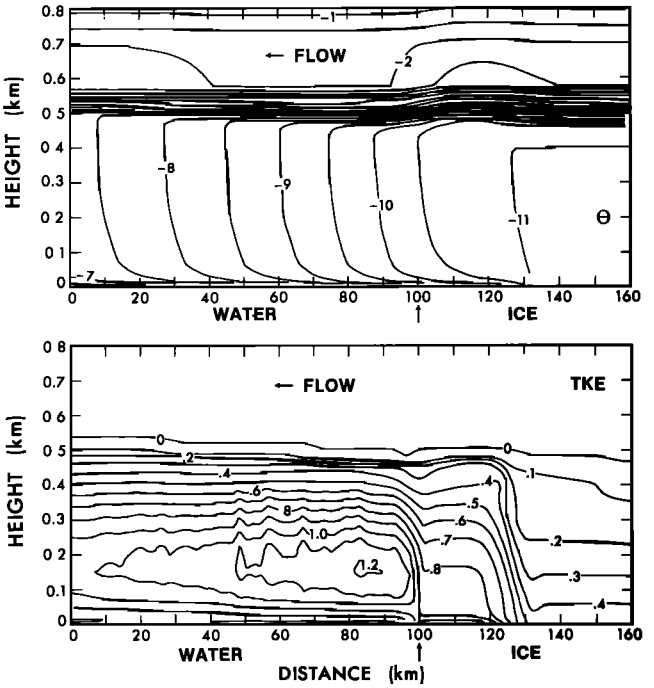

Fig. 6. Potential temperature and turbulence kinetic energy as in Figure 2, but for off-ice winds over the MIZ (case 3; flow from smooth ice across rough ice onto open water). Note the changes in ABL structure across the two transition zones.

most of the ABL. This is due to the fact that the ABL feels the increased roughness of the underlying surface as it flows from open water onto rough ice at the edge of the MIZ. It is also worth noting that the strong acceleration of the ABL winds under on-ice conditions can cause a rapid compaction of the ice pack in the MIZ.

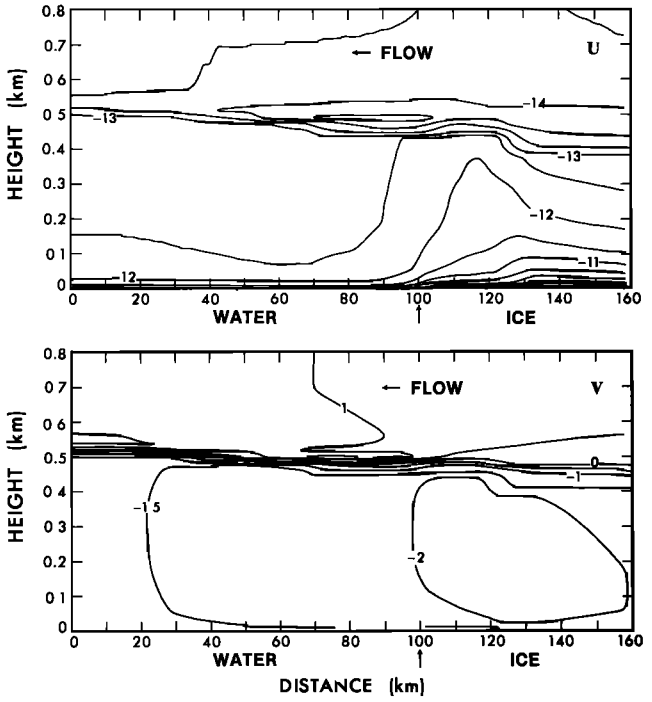

Fig. 7. Cross–ice edge and along–ice edge velocities as in Figure 3, but for off-ice winds over the MIZ (case 3; flow from smooth ice across rough ice onto open water).

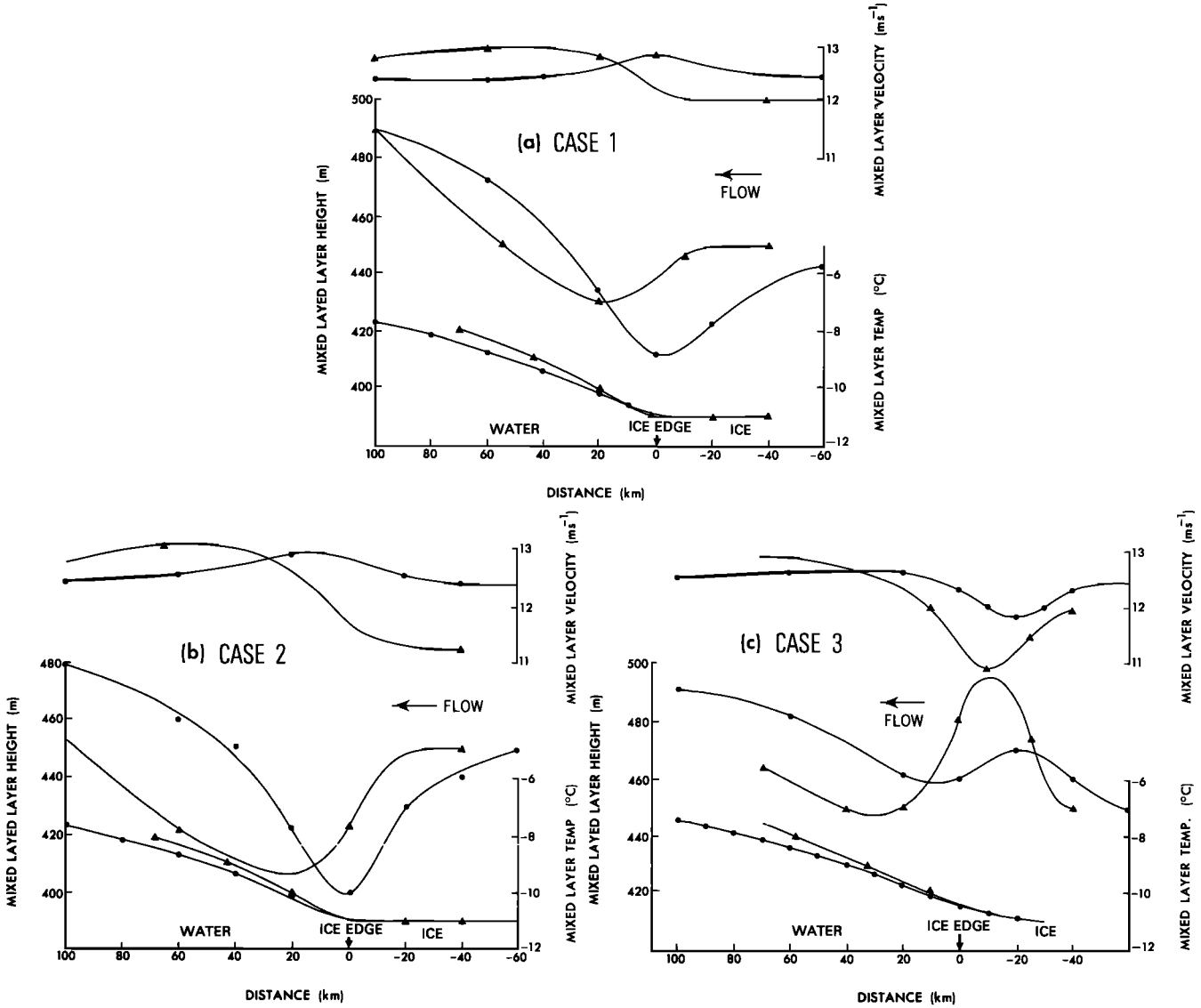

Fig. 8. Mixed layer velocity, mixed layer height, and potential temperature as functions of distance from the ice edge for (*a*) case 1, (*b*) case 2, and (*c*) case 3. The flow is from right to left. Triangles indicate results from the slab model of *Overland et al.* [1983], while circles indicate results of the present model.

Figure 15 shows the cross–ice edge kinematic shear stress as a function of the distance from the ice edge for both cases. The simulation for case 3 once again shows a peak in shear stress due to increased surface roughness, which assists in compacting the ice in the MIZ during on-ice winds but is otherwise of little significance. The ABL adjusts rapidly to the conditions of the underlying surface because of the rapidity with which its turbulence is quenched, since the eddy turnover time scales are only of the order of a few minutes.

The above simulations indicate the dramatic changes possible in the ABL structure when strong heat exchange occurs between the ABL and the ice during on-ice wind conditions. If, however, the heat exchange is not strong, the resulting modifications to ABL structure can be expected to be correspondingly smaller.

On-ice wind conditions over a MIZ are thus clearly substantially different from off-ice conditions and are therefore best simulated by a multilevel model.

4.3. *Along–Ice Edge Wind Conditions*

We present last model simulations of predominantly along–ice edge wind flow conditions; the flow, however, has a small cross–ice edge component (1 m s^{-1}) such that the ABL moves across the ice edge slowly. The ABL is assumed, however, to be in essential equilibrium with the underlying surface initially. Thus its temperature is −11°C over ice and −1°C over open water. The inversion height is the same initially (450 m), and the inversion strength is 12°C over ice and 2°C over the ocean. We consider cases of slow flow both from smooth ice onto open water and vice versa.

When the winds blow essentially along the edge of either a compacted or uncompacted ice pack, at sufficient distance downstream one can expect the air column to be in essential equilibrium with the characteristics of the underlying surface. Thus, for example, the ABL temperature tends to be close to the temperature of the underlying surface, and the turbulence field corresponds to its roughness and is essen-

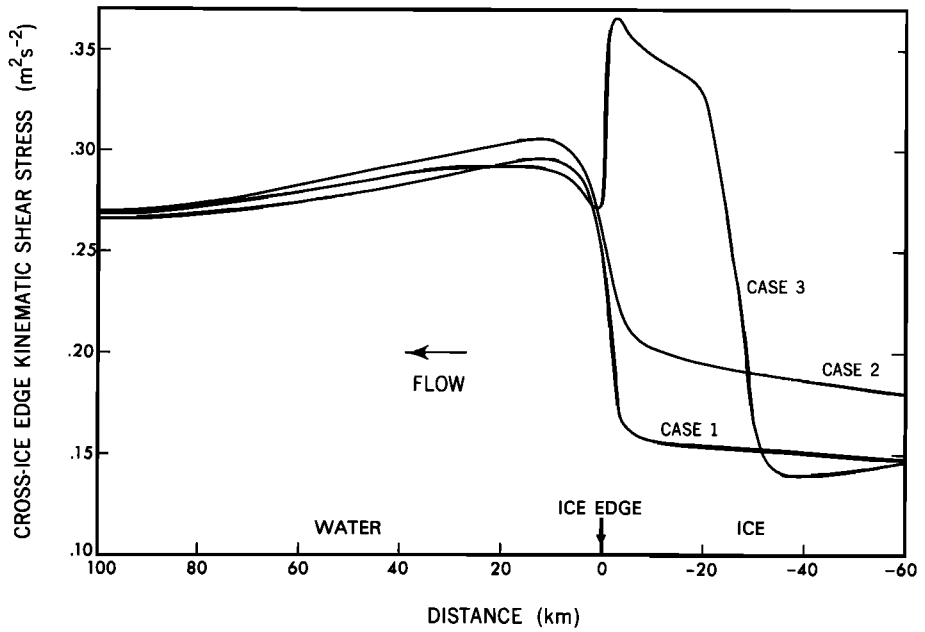

Fig. 9. Cross–ice edge kinematic shear stress at the surface as a function of the distance from the ice edge for all three cases of off-ice wind conditions. Note that the pronounced overshoot in the surface stress for case 3 could lead to ice edge divergence in a MIZ.

tially shear-generated and maintained. Under these conditions, if there results even a small cross–ice edge velocity component, the essentially different air masses over the ice and water begin to interact strongly. Thus, for example, if there is flow from ice onto water, the cold air mass attempts to override the warm one, resulting in overturning and intense turbulence. Figures 16 and 17 show the results of such a simulation. The cross–ice edge component of geostrophic velocity is 1 m s^{-1}. A strong front at the ice edge and the strong turbulence associated with it can be readily seen in Figure 16. The situation is rather analogous to a stationary cold front in the atmosphere. Figure 17 shows the corresponding velocities. Note the strong change in along–ice edge velocities across the inversion over ice.

The opposite situation, where there exists a slow movement of air masses from warm open water onto cold ice is

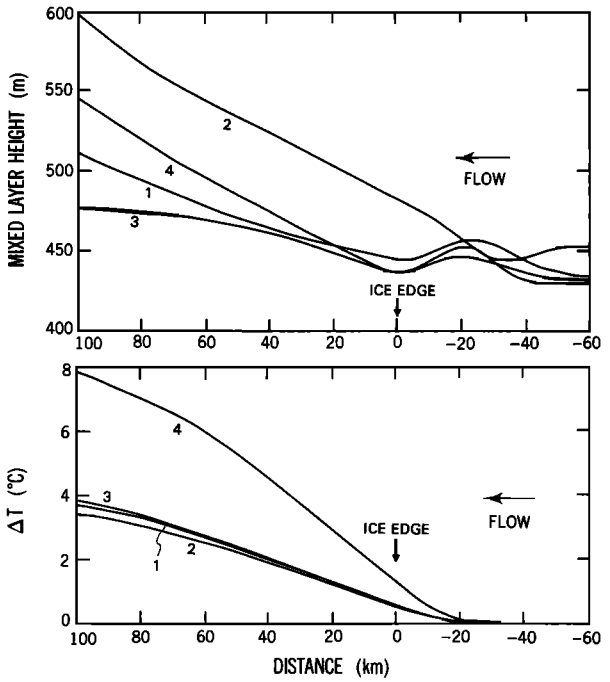

Fig. 10. Mixed layer height and the increase in the mixed layer temperature for four different runs corresponding to case 3. Curve 1 denotes a run with ABL temperature and inversion strength of −11°C and 7°C, respectively; the corresponding values for curves 2, 3, and 4 are −11°C and 2°C, −11°C and 12°C, and −21°C and 7°C, respectively.

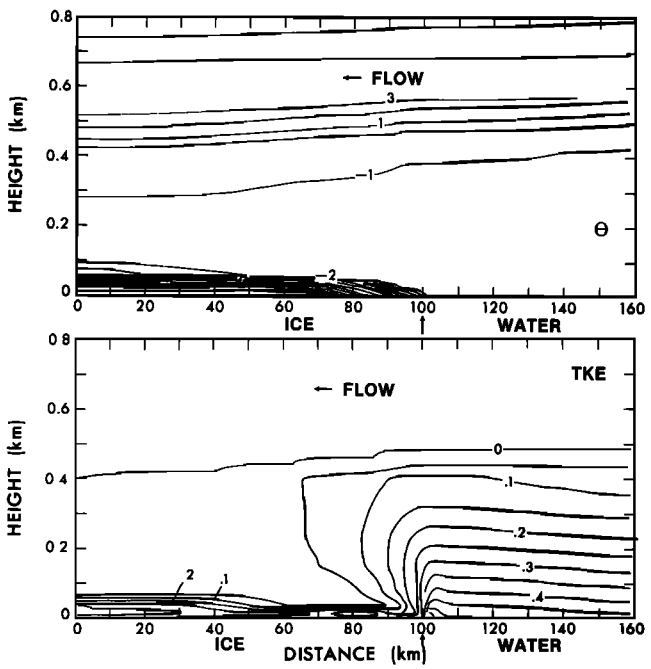

Fig. 11. Potential temperature and turbulence kinetic energy as in Figure 2, but for Case 2 on-ice winds (from open water onto rough ice). Turbulence is strongly suppressed over the ice, and a low-level inversion develops.

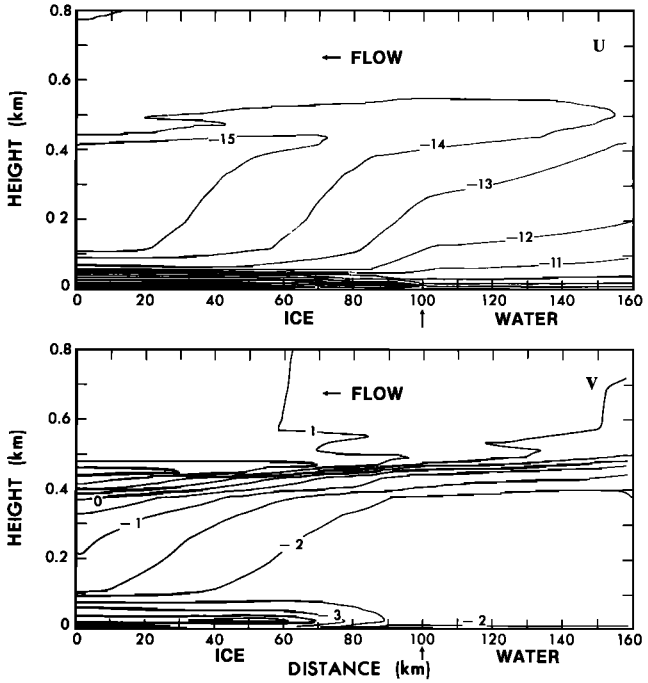

Fig. 12. Cross–ice edge and along–ice edge velocities as in Figure 3, but for case 2 on-ice winds (from open water onto rough ice). Note the strong jet associated with the low-level inversion.

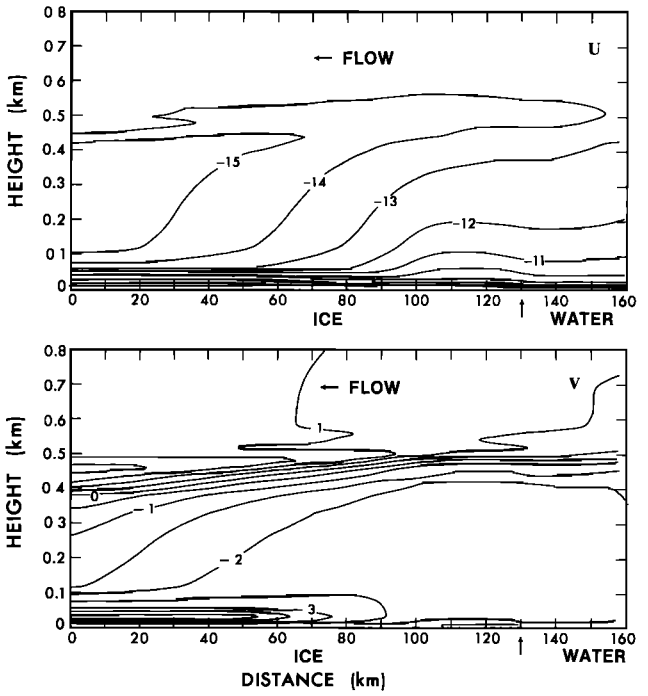

Fig. 14. Cross–ice edge and along–ice edge velocities as in Figure 12, but during on-ice winds over a MIZ (case 3; from open water across rough ice onto smooth ice).

shown in Figures 18 and 19. The inversion height is lowered rather abruptly near the ice edge, and a strong front prevails at the ice edge, as in the previous case. However, the behavior of air masses is slightly different. There now exist two regions of intense turbulence at the ice edge, situated one above the other (Figure 18). There exists a strong shear in the ABL, with flow in the lower layers being from ice onto water, even though above this level, the flow is in concert with the geostrophic winds, i.e., toward the ice (Figure 19). This causes the lower-level cold air masses to override warm ones, resulting in intense turbulence. Above this level, however, the abrupt rise in inversion height produces another region of overturning and intense turbulence. Thus in both cases of essentially along–ice edge flows, the ice edge is associated with a strong thermal front and intense turbulence activity.

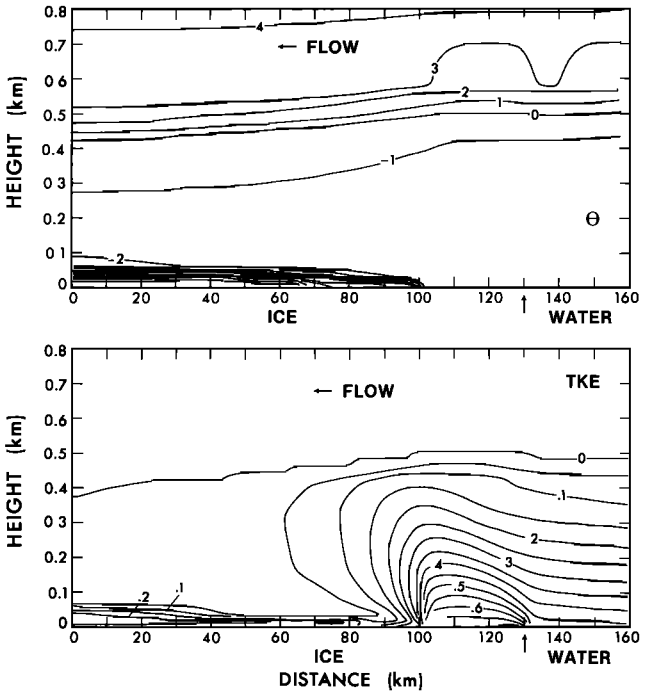

Fig. 13. Potential temperature and turbulence kinetic energy as in Figure 11, but during on-ice winds over a MIZ (case 3; from open water across rough ice onto smooth ice). Turbulence is increased over the MIZ before being suppressed over the interior ice.

5. Concluding Remarks

As the results in the previous section show, the ABL can undergo substantial changes over a MIZ, and the particulars of these changes depend crucially on the flow direction. While there is some observational evidence to at least qualitatively support the model predictions for off-ice conditions, there exist few data to validate the on-ice and along-ice edge simulations. While dramatic changes in ABL structure are certainly possible for these flow conditions, the important issue of the magnitude of heat transfer to the cold ice from the warm ABL remains largely unresolved (but see the following paragraph). It is clear that more model simulations and field observations are essential for a better understanding of the physics of the ABL over a MIZ.

One of the reviewers pointed out that there exists one set of observations that suggests that under on-ice and along–ice edge wind conditions, the ABL over a MIZ is primarily mechanically mixed and no low-level inversions develop. This implies that the heat flux from the warm ABL to the cold ice is negligibly small. In the model simulations also, the turbulence in the ABL is mechanically generated, and if this heat flux were put to zero, the model would also indicate a lack of low-level inversions for on-ice winds. However, it is not clear whether these observations are typical of MIZs or not. This issue clearly needs further study.

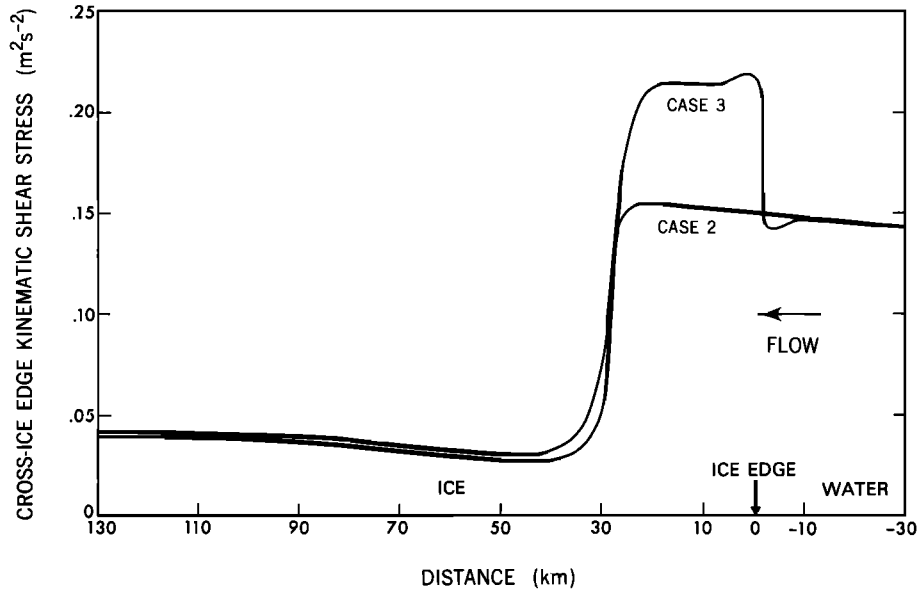

Fig. 15. Cross-ice edge kinematic shear stress at the surface as a function of the distance from the ice edge for both cases of on-ice wind conditions.

While a satellite picture of off-ice winds over a MIZ illustrates one of the more dramatic atmospheric phenomena captured by remote sensing, other flow directions might be equally significant in terms of their effects on the ABL. It is also clear that because the changes in the ABL across a MIZ could be strong, it is advisable to account for these effects in understanding and modeling the ocean and the ice cover in these regions. In this paper we have prescribed the conditions of the underlying surface and held them fixed while concentrating on the changes in the ABL structure. Thus we have ignored the feedback between the ice-ocean medium and the ABL. This feedback should lead to a further enrichment of the exchange processes and is best studied through a coupled model of the atmosphere-ice-ocean system. Fortunately, because of several ongoing observational efforts such as the Coordinated Eastern Arctic Experiment (CEAREX), the coupling of all three mediums is being

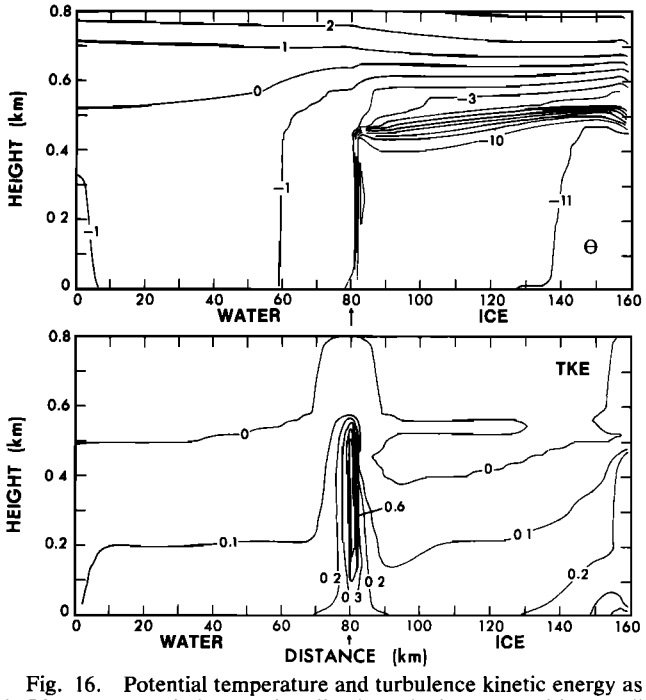

Fig. 16. Potential temperature and turbulence kinetic energy as in Figure 2, but winds are primarily along the ice edge, with a small geostrophic component from right to left, from ice onto open water. The ice surface is smooth. Note the strong front associated with the ice edge and the intense turbulence there due to rapid mixing of the air masses.

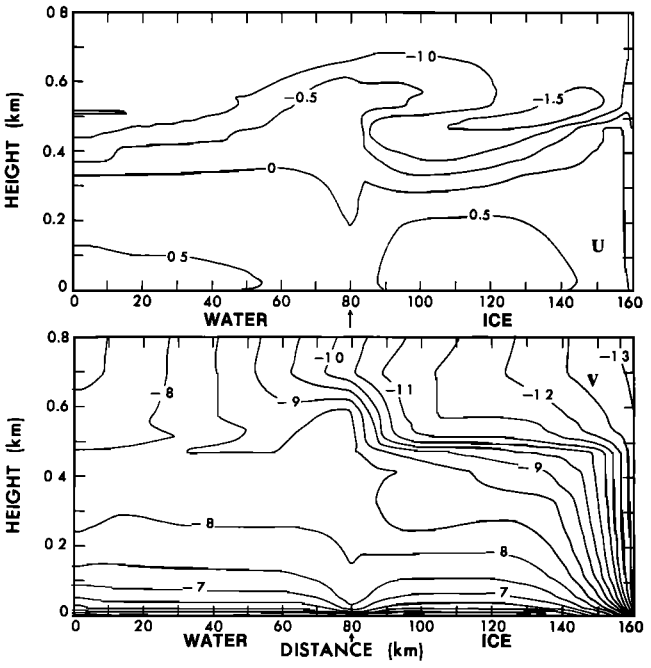

Fig. 17. Cross-ice edge and along-ice edge velocities as in Figure 3, but winds are primarily along the ice edge, with a small geostrophic component from right to left, from ice onto open water. The ice surface is smooth. Note the strong shear across the inversion over ice.

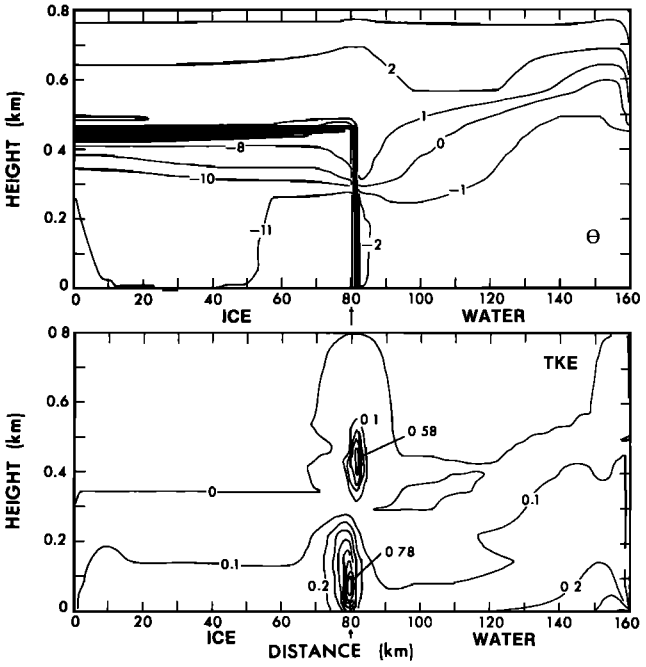

Fig. 18. Potential temperature and turbulence kinetic energy as in Figure 16; winds are primarily along the ice edge, with a small geostrophic component from right to left, but from open water onto ice. The ice surface is smooth. Note the strong front associated with the ice edge and the intense turbulence there due to rapid mixing of the air masses.

intensively studied. The coming years should see a substantial improvement in our understanding of marginal ice zones and provide a better data base for the development of truly coupled models of the atmosphere, ice, and the ocean.

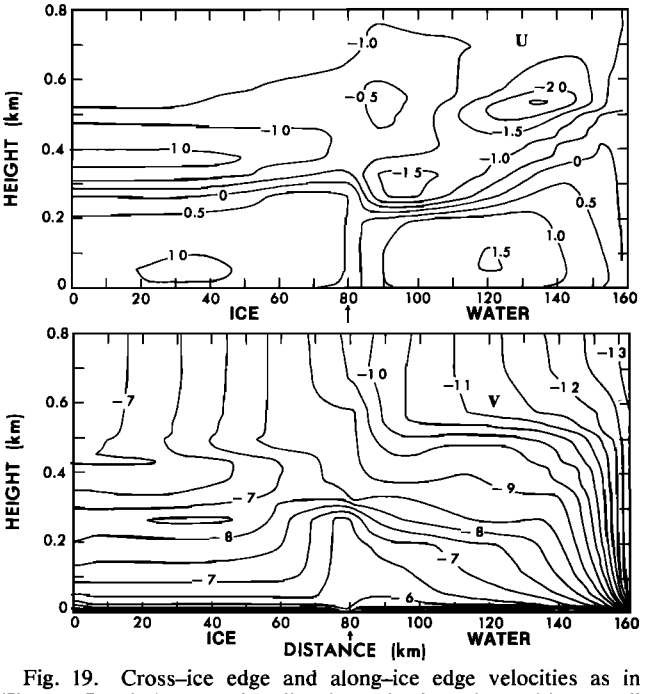

Fig. 19. Cross-ice edge and along-ice edge velocities as in Figure 17; winds are primarily along the ice edge, with a small geostrophic component from right to left but from open water onto ice. The ice surface is smooth. Note the wind reversal around 275 m height.

Acknowledgments. L.H.K. acknowledges with great pleasure the encouragement of James Overland and Carol Pease. L.H.K. was supported by Office of Naval Research under grant ONR-N00014-86-C-0438 (through Dynalysis of Princeton), and G.L.M. was supported under ONR-N00014-84-K-0-0640. L.H.K. appreciates the warm hospitality of the Geophysical Fluid Dynamics Laboratory (GFDL) during the course of this work and thanks Phil Tunison and Jeff Varanyak of GFDL for drafting the figures.

REFERENCES

Anderson, R. J., Wind stress measurements over rough ice during the 1984 Marginal Ice Zone Experiment, *J. Geophys. Res.*, *92*, 6933–6941, 1987.

Andreas, E. L., W. B. Tucker III, and S. F. Ackley, Atmospheric boundary-layer modification, drag coefficient, and surface heat flux in the Antarctic marginal ice zone, *J. Geophys. Res.*, *89*, 649–661, 1984.

Bennett, T. J., Jr., and K. Hunkins, Atmospheric boundary layer modification in the marginal ice zone, *J. Geophys. Res.*, *91*, 13,033–13,044, 1986.

Blumberg, A. F., and G. L. Mellor, Diagnostic and prognostic numerical circulation studies of the South Atlantic Bight, *J. Geophys. Res.*, *88*, 4579–4592, 1983.

Blumberg, A. F., and G. L. Mellor, A description of a three-dimensional coastal ocean circulation model, in *Three-Dimensional Coastal Ocean Models*, *Coastal and Estuarine Sci.*, vol. 4, pp. 1–16, AGU, Washington, D. C., 1987.

Guest, P. S., and K. L. Davidson, The effect of observed ice conditions on the drag coefficient in the summer East Greenland Sea marginal ice zone, *J. Geophys. Res.*, *92*, 6943–6954, 1987.

Kantha, L. H., and G. L. Mellor, A two-dimensional coupled ice-ocean model of the Bering Sea marginal ice zone, *J. Geophys. Res.*, in press, 1989.

Kellner, G., C. Wamser, and R. A. Brown, An observation of the planetary boundary layer in the marginal ice zone, *J. Geophys. Res.*, *92*, 6955–6965, 1987.

Markatos, N. C., The mathematical modelling of turbulent flows, *Appl. Math. Model.*, *10*, 190–220, 1986.

McPhee, M. G., Turbulent heat and momentum transfer in the oceanic boundary layer under melting pack ice, *J. Geophys. Res.*, *88*, 2827–2835, 1983.

Mellor, G. L., and L. H. Kantha, A coupled ice-ocean model, in press, *J. Geophys. Res.*, 1989.

Mellor, G. L., and T. Yamada, Development of a turbulence closure model for geophysical fluid problems, *Rev. Geophys.*, *20*, 851–875, 1982.

Oey, L.-Y., G. L. Mellor, and R. I. Hires, A three-dimensional simulation of the Hudson-Raritan estuary, 1, Description of the model and model simulations, *J. Phys. Oceanogr.*, *15*, 1676–1692, 1985.

Overland, J. E., Atmospheric boundary layer structure and drag coefficients over sea ice, *J. Geophys. Res.*, *90*, 9029–9049, 1985.

Overland, J. E., A model of the atmospheric boundary layer over sea ice during winter, paper presented at the Conference on Polar Meteorology and Oceanography, Am. Meteorol. Soc., Madison, Wis., March 19–22, 1988.

Overland, J. E., R. M. Reynolds, and C. H. Pease, A model of the atmospheric boundary layer over the marginal ice zone, *J. Geophys. Res.*, *88*, 2836–2840, 1983.

Reynolds, M., On the local meteorology at the marginal ice zone of the Bering Sea, *J. Geophys. Res.*, *89*, 6515–6524, 1984.

Rodi, W., Examples of calculation methods for flow and mixing in stratified fluids, *J. Geophys. Res.*, *92*, 5305–5328, 1987.

L. H. Kantha, Institute for Naval Oceanography, Stennis Space Center, MS 39529.

G. L. Mellor, Atmospheric and Oceanic Sciences Program, Princeton University, Princeton, NJ 08544.

(Received June 6, 1988;
revised January 10, 1989;
accepted August 30, 1988.)